Engineering fluorescent reporters in human pluripotent cells and strategies for live imaging human neurogenesis

Alwyn Dady*[1], Lindsay Davidson, Nicolas Loyer, Timothy Sanders[2], Jens Januschke & Kate G. Storey*

Division of Molecular, Cell & Developmental Biology, School of Life Sciences, University of Dundee, Dundee DD1 5EH, UK

* co-corresponding authors

[1] current position: Université Paris Est Créteil (UPEC), Glycobiology, Cell Growth and Tissue Repair Research Unit (Gly-CRRET), F-94010 Créteil, France

[2]University of California, San Francisco, Benioff Children's Hospital Oakland, USA

Running title: human PSC reporters for live imaging

Key words: human pluripotent cells, human spinal cord development, human cortical development, live cell imaging, piggyBac-mediated fluorescent reporters

Abstract

Investigation of cell behaviour and cell biological processes in human embryonic tissues is facilitated by creation of fluorescent reporters in human pluripotent stem cell lines, which can be differentiated into cell types of choice. Here we report use of a piggyBac transposon-mediated stable integration strategy to engineer human pluripotent stem cell reporter lines. These express a plasma membrane (pm) localised protein tagged with the fluorescent protein eGFP or mKate2, the photoconvertible nuclear marker H2B-mEos3.2, with or without pm-mKate2, and the cytoskeletal protein F-tractin tagged with mKate2. Focussing on neural development some of these lines were used to live image and quantify cell behaviours, including cell cycle progression and cell division orientation in spinal cord rosettes. Further, lipofection-mediated introduction of piggyBac constructs into human neural progenitors labelled single cells and small cell groups within rosettes, allowed monitoring of individual cell behaviours including neuronal delamination. Finally, using the F-tractin-mKate2 hiPSC line, actin dynamics were captured during proliferation in cortical neural rosettes. This study presents new tools and techniques with which to interrogate human cell behaviour and cell biology using live imaging approaches.

Introduction

Live imaging is used to monitor the behaviour of cells within tissues and to reveal sub-cellular proteins dynamics. This includes important cellular processes such as cell cycle progression and changes in cell shape and adhesion as individual cells differentiate and cells group together to form structures during tissue morphogenesis. Such approaches provide insight into developmental and tissue homeostasis mechanisms and elucidate changes in disease states. The ability to genetically engineer human pluripotent stem cells to express fluorescent proteins facilitates such live imaging approaches and allows high resolution investigation of cell behaviour and cell biological processes in human tissue models.

DNA constructs can be introduced into human pluripotent cells in numerous ways. The piggyBac transposon system has advantages compared to other stable integration approaches, particularly for live cell imaging studies. In comparison with viral vectors, such as adenovirus or lentivirus (Lee, et al., 2017), the piggyBac system is more secure and convenient to generate (Ding, et al., 2005, Wang, et al., 2008, Woltjen, et al., 2009). Viral integration sites are non-random but diverse and there is no control over copy number and gene expression levels, (Cereseto and Giacca, 2004, Engelman, 2003, Sultana, et al., 2017): indeed viral integrations can alter endogenous gene expression, including vital regulatory genes and/or inactivation of tumour-suppressor genes, impacting cell behaviour and differentiation (e.g. (Hacein-Bey-Abina, et al., 2010, Hacein-Bey-Abina, et al., 2003). In contrast, piggyBac constructs flanked by a 13bp perfect terminal invert repeat sequence insert specifically into P-elements (TTAA segments) in the genome (Elick, et al., 1996, Lee, et al., 2011, Liu, et al., 2013). Other transposon systems are also used including hAT-Tol2, (Kawakami, 2007, Kawakami and Shima, 1999) or Tcl-like transposons, *Sleeping Beauty* and *Frog Prince*, (Ivics, et al., 1997, Miskey, et al., 2003, Narayanavari, et al., 2017). However, while *Sleeping Beauty* and piggyBac have the highest transposition activity in mammalian cells (Kim and Pyykko, 2011), *Sleeping Beauty* is less reliable, with a tendency for local hopping and leaving a CAG footprint following excision (Wang, et al., 2008, Wu, et al., 2006).

In comparison with other stable integration approaches, Transcription Activator-like Effector Nucleases (TALENs) (Hockemeyer, et al., 2011, Joung and Sander, 2013, Miller, et al., 2011, Wood, et al., 2011) and CRISPR/Cas9 (Charpentier and Doudna, 2013, Doudna and Charpentier, 2014, Jinek, et al., 2012, Pacesa, et al., 2024), which achieve precision gene engineering of single copy insertions at a defined locus, the piggyBac transposon system will insert multiple copies of fluorescently tagged proteins within the many P-elements/ TTAA chromosome sites (Elick, et al., 1996, Lee, et al., 2011) (Liu, et al., 2013, Woodard and Wilson,

116 2015). This feature of the piggyBac system has a particular advantage for long term live-imaging
117 by increasing transgene copy number and expression, and so detection sensitivity for
118 fluorescently tagged proteins. This in turn reduces exposure times and thereby potential
119 phototoxicity.

120 Nevertheless, gene editing using CRISPR/Cas9 and other nucleases has been
121 successfully used to express fluorescently tagged endogenous proteins for live cell imaging
122 (Dambournet, et al., 2014) and these include hiPSC lines expressing, for example, mEGFP-
123 nuclear lamin B1 (Haupt, et al., 2018, Roberts, et al., 2017). This has the advantage of
124 endogenous regulatory control of fusion protein expression but does rely on this having
125 sufficient strength for live detection and for longer term live cell imaging. Fusion of an
126 endogenous protein with large exogenous sequences such as GFP may also compromise
127 protein function. Indeed, such approaches typically report low recovery of biallelic edits, which
128 may reflect lack of tolerance for two tagged copies of an indispensable protein, but this is likely
129 to be protein specific (Roberts, et al., 2017). Inclusion of an amino acid linker sequence
130 between the native and fluorescent protein can mitigate this risk. Such engineered hPSC lines
131 require quality controls, including confirmation of pluripotency, karyotype and growth rate as
132 well as comparison with endogenous protein localisation and cell behaviour in well-defined
133 differentiation assays.

134 Here we describe use of a piggyBac mediated engineering strategy to create a series of
135 human pluripotent stem cell reporter lines by introducing fluorescent proteins which localise
136 to the plasma-membrane, chromatin, or actin cytoskeleton. We characterise these lines and
137 deploy them, or lipofected piggyBac constructs introduced during differentiation, in live
138 imaging protocols to uncover fundamental characteristics of human neural progenitor cell
139 behaviour in *in vitro* assays for spinal cord and cerebral cortex development.
140

141 Results and Discussion

142

143 Generation of human pluripotent cell fluorescent reporter lines using the piggyBac-
144 transposon stable integration system

145 To facilitate analysis of cell behaviour in live tissue derived from human pluripotent stem cells
146 we generated a series of fluorescent reporter hESC or iPSC lines (Dady, et al., 2022)(Figures
147 1A,B). To monitor cell shape and dynamics we used a plasma membrane (pm) localised protein
148 tagged with eGFP or mKate2 (pm-eGFP or pm-mKate2) (Sanders, et al., 2013). To allow
149 monitoring of the cell nucleus we engineered a line expressing H2B-mEos3.2, the latter
150 localising in the nucleus and mEos3.2 having the potential for laser-mediated photo-conversion
151 (Zhang, et al., 2012) and so the labelling and tracking of individually selected cells. This provides
152 the potential for clonal analysis in combination with immunofluorescence for cell type specific
153 marker proteins. We also co-transfected H2B-mEos3.2 and pm-mKate2 expressing plasmids to
154 allow monitoring of labelled nuclei and changes in cell shape. Finally, to monitor actin
155 cytoskeletal dynamics we created an F-tractin-mKate2 cell line.

156 To generate these reporters, we used the hESC line H9 (for pm-eGFP, pm-mKate2,
157 H2B-mEos3.2), or hiPSC line ChiPS4 for F-Tractin-mKate2 and a further pm-eGFP line (Dady, et
158 al., 2022) and we deployed the piggyBac transposon-mediated stable integration strategy
159 (Sanders, et al., 2013, Sarkar, et al., 2003, Yusa, et al., 2009, Yusa, et al., 2011). The piggyBac
160 vectors are composed of the specific fusion protein of interest whose expression is driven by a
161 CAG promoter (Figures 1A,B). This cargo is then flanked by two Inverted Terminal Repeat (ITR)
162 sequences which allow a hyperactive piggyBac transposase (HyPBase, characterised by highly
163 stable enzymatic activity), to cut and paste the cargo within the specific TTAA-chromosomal
164 sites (Yusa, et al., 2011). Critical to efficient stable integration was transfection of 5 times more
165 piggyBac vector than transposase.

166 The cloning strategy for generating these constructs is described in the Methods. Once
167 complete these were introduced to a suspension of $1x10^6$ hPSCs by electroporation with a final
168 concentration of 1.2 µg/µl of piggyBac constructs and HyPBase (Yusa, et al., 2011) (Figures 1C
169 Methods). Transfected hPSCs were then FAC-sorted and selected using their specific
170 fluorescence properties: this optimized protocol delivered a high rate of transfection (Figure
171 S1). Using this approach, polyclonal cell lines were generated for each fusion protein of
172 interest: these were composed of cells with this construct randomly inserted within each
173 genome. Polyclonal lines were sorted with easily detectable, but not high, fluorescence for live
174 imaging studies. We also made a monoclonal line for pm-eGFP in ChiPS4 for future use as this

175 approach would obviate the remote possibility of cell-to-cell variation impacting cell behaviours
176 captured in live imaging experiments (Figure 1D).
177
178 Using human pluripotent cell fluorescent reporter lines to monitor and quantify cell behaviour
179 in human spinal cord rosettes
180 These fluorescent reporter hPSC lines allowed the development of *in vitro* assays for monitoring
181 and quantifying human cell behaviour. Here we first focussed on capturing fundamental
182 parameters of human neurogenesis using our established spinal cord rosette assay (Dady, et
183 al., 2022, Verrier, et al., 2018)(Figure 2A). This involves differentiating hPSCs into Neuro-
184 Mesodermal Progenitor-like cells (NMP-like cells) and their subsequent differentiation into
185 SOX2 expressing neural progenitors, which self-organise into neural rosettes exhibiting
186 localised expression of apico-basal polarity markers such as NCAD/CDH2 by Day 6 (D6) following
187 NMP-L cell plating (Dady, et al., 2022). This differentiation assay generates neural crest
188 progenitors and dorsal neural progenitors, with the first neurons apparent from D8, peak
189 neurogenesis at D14 and gliogenesis onset by ~ D20. This sequence of events is in line with
190 those documented in the human embryonic spinal cord with dorsal neurogenesis at forelimb
191 level commencing by CS12/13 and gliogenesis by CS18 (Dady, et al., 2022, Rayon, et al., 2020).
192 The cell lines expressing pm-eGFP and pm-mKate with H2B-mEos3.2 lend themselves
193 to analysis of cell shape change. We wished to monitor the dynamics of neuroepithelial cell
194 behaviour as these cells progressed through the cell cycle during inter-kinetic nuclear migration
195 (IKNM)(Sauer, 1935, Spear and Erickson, 2012). This behaviour is characteristic of pseudo-
196 stratified epithelia and involves movement of the nucleus from the basal to the apical side of a
197 cell in G2 phase, subsequent mitosis at the apical (ventricular) surface and return to the basal
198 surface in G1: here a neuroepithelial cell may then either re-enter S-phase or exit the cell cycle
199 and commence neuronal differentiation. To monitor this behaviour in spinal cord rosettes we
200 first optimised our assay to address a major challenge of longer-term live imaging, increasing
201 thickness of the developing tissue over time (D6 rosettes are typically ~ 100µm). This reduces
202 the ability to maintain cells of interest in focus, even when deploying a long working-distance
203 lens and deconvolution algorithms (see Methods). To reduce the thickness of rosettes we
204 developed a re-plating regime in which D6 rosettes were manually micro-dissected and
205 replated on glass-bottom dishes suitable for microscopy (Figure 2B). This resulted in formation
206 of small satellite micro-rosettes (SmR) surrounding the replated primary rosette (PrR) (Figure
207 2C). Satellite micro-rosettes were polarised as indicated by apical actin localisation. Most

208 importantly, SmR were flatter (~ 50µm thick) allowing longer term high-resolution live cell
209 imaging.
210 Human spinal cord satellite rosette cells derived from hESCs expressing pm-eGFP or
211 pm-mKate and H2B-mEos3.2 were then imaged at intervals for 24h at D13-D14 and at D18-D19
212 (Figs. 2D-E, movie 1). Apical visiting time (defined as the period during which a basally located
213 nucleus transits to the apical surface, divides and returns to a basal position) and used as an
214 indication of changing cell cycle duration, increased from D13/D14 to D18/D19 and
215 approximately doubled over this 6-day period (D13, 11h ± 3h; D19, 25h ± 7h (Fig. 2F). This real
216 time measurement confirmed that cell cycle time extends as human ESC derived spinal cord
217 progenitors age (Rayon, et al., 2020). These findings further correlate with studies in mouse
218 (Calegari, et al., 2005, Calegari and Huttner, 2003, Takahashi, et al., 1995), and chick (Olivera-
219 Martinez, et al., 2014) embryos showing that neuron-generating divisions, which appear later
220 in development, are characterized by longer IKNM and cell cycle duration.
221
222 Labelling and live-imaging individual human spinal cord rosette cells using temporally defined
223 lipofection of piggyBac constructs
224 While it is possible to follow individual cell profiles as pm-FP expressing cells approach the
225 apical surface, divide and return to a basal position we also wished to monitor sub-cellular
226 behaviour within individual cells, including mitotic spindle orientation and final cleavage plane
227 as well as cell delamination events within this human neuroepithelium. To achieve this, we
228 designed a new strategy taking advantage of the precise timing of neurogenesis (Fig. 2A) (Dady,
229 et al., 2022) and a less efficient mode of cell transfection (Fig.3A): a mixture of piggyBac
230 constructs and the HyPBase transposase was transfected into D8/D9 human spinal cord neural
231 progenitors using lipofection (Felgner, et al., 1987)(Figure 3A, see Methods). Lipofected
232 neurogenic neural rosettes were then allowed to differentiate to later stages (Fig.3A). This
233 approach led to labelling of single or small groups of human spinal cord progenitors within each
234 rosette (Figs.3B,C).
235 Lipofection of cells with the pm-mKate and H2B-mEos3.2 plasmids allowed us to
236 monitor cell shape and chromatin configuration and so facilitated analysis of the orientation of
237 the mitotic spindle and final cleavage plane. Rosettes containing such cells were cultured until
238 D13 or D18 and imaged at 10 min intervals for 24-30h. Most divisions within each rosette
239 between D13 and D14 were symmetrical, with vertical cleavage planes and resulting horizontal
240 divisions, while between D18 and D19 most divisions were asymmetric, with horizontal
241 cleavage planes and resulting vertically orientated divisions (Figs 3D-F, movie 3). These findings

242 demonstrate that division orientation alters as development proceeds in human spinal cord
243 neuroepithelium. This change correlates with the longer apical visiting times and the
244 accumulation of neurons in later stage rosettes (Dady, et al., 2022).
245 To monitor delamination of new-born neurons within rosettes we followed individual
246 cells with a basally located nucleus and a long cellular process inserted into the apical surface
247 of the rosette. In a subset of these cells, we were able to observe delamination from the apical
248 surface, a step characteristic of new-born neurons (Das and Storey, 2014). Moreover, this
249 involved the abscission of an apical membrane particle in a manner characteristic of the apical
250 abscission mechanism first found in the chicken spinal cord (Das and Storey, 2014, Kasioulis, et
251 al., 2017)(Fig. 3G, 3H and movie 5). Overall, these analyses of human neuroepithelial cell
252 behaviour during differentiation revealed the expansion of the early human neural progenitor
253 cell pool in developing spinal cord, followed by a later phase characterized by slower cell cycle
254 progression, increased asymmetric cell division and the generation of neurons.
255
256 Live imaging F-tractin in human cerebral cortex progenitors uncovers known and novel actin
257 dynamics
258 Filamentous actin is a fundamental cytoskeletal component involved in the mechanics of cell
259 division, cell motility and force transduction within tissues, and recent work has further
260 uncovered roles around (Davidson and Cadot, 2021) and within the nucleus (Gunasekaran, et
261 al., 2022, Hyrskyluoto and Vartiainen, 2020) where actin regulates gene expression as part of
262 the nucleoskeleton in cell type and cell state specific ways, e.g. (Okuno, et al., 2020). Within
263 the developing vertebrate neuroepithelium dynamic actin mediates aspects of IKNM (Spear
264 and Erickson, 2012, Yanakieva, et al., 2019), apical cell adhesion and constriction leading to
265 neuronal delamination, as well as intercellular filopodial contacts between non-neighbouring
266 cells, e.g. (Das and Storey, 2014, Kasioulis, et al., 2022, Kasioulis, et al., 2017). In humans, actin
267 cytoskeleton dysfunction in the cerebral cortex leads to periventricular heterotopia
268 characterised by failure of neuronal delamination, altered cell adhesion and reduced brain
269 size/cell proliferation, and is associated with seizures, dyslexia and psychiatric disorders (Lian
270 and Sheen, 2015). Periventricular heterotopia is linked to mutation of actin binding proteins
271 such as Filamin A (Sheen, et al., 2005). Moreover, the uniquely human fusion gene *CHRFAM7A*
272 acts at least in part by activating actin in neuronal progenitors, impacting cell shape, growth
273 cone extension and dendritic spine formation and so synaptic clustering (Szigeti, et al., 2023).
274 The mechanisms by which actin mediates such critical processes in the developing human brain
275 have yet to be elucidated.

276 The F-tractin-mKate2 hiPSC line was used to capture detailed actin dynamics in
277 cerebral cortex (cortical) neural rosettes. A dual-SMAD forebrain differentiation protocol was
278 followed, after (Chambers, et al., 2009) and neuroepithelial rosette structures were generated
279 by day 28. The appearance of Tbr2/EOMES positive cells (Fig. S2A) indicated that some basal
280 progenitors were present and confirmed forebrain tissue identity, while Beta-Tubulin labelling
281 (Fig. S2B) established neuron generation. Live imaging analyses focussed on actin dynamics in
282 cell behaviours characteristic of early cortical development. F-Tractin localised as expected to
283 the neuroepithelial cell cortex and was enriched at the apical cell junctions around apical end
284 feet and in rounding mitotic cells (Fig. 4A and movie 4): a similar distribution was revealed by
285 Phalloidin staining of fixed rosettes (Fig S2C). Apical enrichment of F-Tractin was also observed
286 during cell delamination from the apical surface (Fig 4B, movie 5). F-Tractin was detected at
287 low levels in the cytoplasm, distinguishing the nucleus (where F-Tractin was not detected) and
288 nuclear envelope breakdown (NEB) (Figs 4C-E). Most divisions (97%) took place at the apical
289 surface; 92% were symmetrical with a vertical cleavage plane (Fig. 4C, movie 6), while the
290 remaining divisions were asymmetric with a horizontal cleavage (Fig. 4D, movie 7). A few basal
291 divisions within the plane of rosettes (Fig. S2D, movie 8) correlated with low numbers of Tbr2
292 expressing cells at this time (Fig. S2A).
293 Focussing on entry into prophase, a transient F-Tractin enrichment localised to the
294 basal nuclear membrane prior to NEB: this was never observed on the apical side of the nuclear
295 membrane and disappeared as soon as NEB occurred (7.8±2.8' later, Fig 4C, and Fig 4E, 5'). This
296 pattern of actin localisation is a novel observation, which to the best of our knowledge has not
297 been described before. Actin polymerises around the entire nuclear envelope of mitotic U2OS
298 human cells just prior to NEB and associates with nuclear envelope remnants to facilitate
299 chromosome congression and correct segregation (Booth, et al., 2019). We speculate that, in
300 cortical progenitor cells, polarised actin polymerisation at the basal nuclear surface may
301 similarly prevent basal chromosome displacement and enable apically localised mitosis.
302 Following NEB, a strong enrichment of F-Tractin was further observed in the bulk of the basal
303 cortex as it moved toward the apical surface (Figs 4C-E). This movement ended 15.6±5.2' after
304 NEB (Fig 4C) with the cell rounding at the apical surface. At this stage, a thin basal process
305 persisted (Fig 4C, 26') and cytokinesis occurred 12.4±6.1' later. A role for actin in apical nuclear
306 movement during IKNM has been reported in the vertebrate neuroepithelium (Norden, et al.,
307 2009, Spear and Erickson, 2012, Yanakieva, et al., 2019) and in *Drosophila* larval wing disk cells,
308 where perturbation of actin polymerisation in the basal process disrupted apical movement
309 during IKNM (Meyer, et al., 2011). Overall, this analysis of F-tractin localisation in human

310 cortical rosettes revealed novel (accumulation at the basal nuclear membrane) as well as
311 expected actin localisations and dynamics. Next steps might include identification of actin
312 binding proteins that regulate specific actin functions and development of this tool to include
313 a nuclear localisation signal to investigate the roles of nuclear actin.
314
315 The human pluripotent fluorescent protein reporter cell lines generated and
316 characterised here and the piggyBac strategy used to generate such reporters, will be valuable
317 for the investigation of the cell biology of human neurogenesis. This could be extended from
318 neural rosettes to brain organoids to elucidate mechanisms underlying human cortical
319 expansion and indeed to any cell or tissue type that can be differentiated from these
320 pluripotent cell lines. Such tissue assays could be used to screen for the impact of
321 environmental factors (e.g. extreme heat, toxins, and other stressors) on human cell behaviour
322 and differentiation. The ability to visualise the actin cytoskeleton and other key cell biological
323 elements in pluripotent cells and their derivatives may also pave the way for biomechanical
324 studies in human tissues. These reporter cell lines could also be used in combination with
325 pharmacological studies, chemical genetics approaches, or in functional assays involving acute
326 and targeted degradation of proteins using proteolysis targeting chimeras (PROTACs) to
327 elucidate molecular mechanisms underlying cellular and developmental processes.

Materials and Methods

Human pluripotent cell authentication and quality control

Human ESC line H9 was obtained from WiCell and human iPSC line ChiPS4 from Cellartis AB, now Takara Bio Europe. These suppliers provided documentation confirming cell identity. STR DNA profiling for ChiPS4 and ChiPS4-pmGFP (polyclonal), H9 (WA09) confirmed identity of these lines in our laboratory. All cell lines were expanded and banked on arrival. Prior to experiments representative lots of each cell bank were thawed and tested for post-thaw viability and to ensure sterility and absence of mycoplasma contamination. Sterility testing was performed by direct inoculation of conditioned medium into tryptic soya broth and soya bean casein broth and no contamination was observed. Mycoplasma testing was carried out by DAPI staining of fixed cultures and using the mycoalert mycoplasma detection kit (Lonza). We confirm that the cell lines used in this study were free of mycoplasma and aerobic bacteria and fungi.

H9 (WA09) hES cells were supplied at passage 24, the cells were thawed, and cell banks prepared at passage 29: for experiments the cells were used between passage 31 and 41. ChiPS4 hiPS cells were supplied at passage 9 and cell banks prepared at passage 13: for experiments the cells were used between passage 15 and 25. Two passages after thawing cells were checked for uniform expression of pluripotency markers (OCT4, SOX2, NANOG, SSEA-3, SSEA-4 TRA-1-60 and TRA-1-81), absence of differentiation markers (SSEA-1, HNF3-beta, beta-III-tubulin and smooth muscle alpha actinin) by immunofluorescence.

Human Pluripotent cell culture

Human pluripotent stem cells were maintained as feeder-free cultures in TESR medium (Ludwig, et al., 2006) supplemented with bFGF (30ng/mL, Peprotech) and Noggin (10ng/ml, Peprotech) on Geltrex matrix coated plates (10 $\mu g/cm^2$, Life Technologies) at 37^oC in a humidified atmosphere of 5% CO_2 in air. Cells were enzymatically dispersed twice a week using TrypLE select (Life Technologies), counted using a hemacytometer and seeded on Geltrex coated plates at a density of 3e4-5e4 cells/cm^2. For single-cell passaging, the medium was supplemented by addition of the Rho kinase inhibitor Y-27632 (10 μM, Tocris). All work with hESCs was undertaken in accordance with the UK Stem Cell Bank steering committee (license number SCSC14-29).

363 Plasmid expression constructs

364 The APX1 (Advanced PiggyBac Expression) plasmid was synthetically engineered to harbor
365 improved PiggyBac inverted terminal repeats (ITRs), the cytomegalovirus (CMV)
366 enhancer/chicken Beta-actin (CAG) promoter, woodchuck post regulatory element (WPRE),
367 and the Life Technologies Gateway recombination cassette allowing for efficient phiC31-
368 mediated recombination (Sanders, et al., 2013)(Figure 1A). Subcellularly localized fluorescent
369 protein gene cassettes were synthesized by overlap extension PCR and cloned into the Gateway
370 Entry Vector, pENTRDTOPO, sequence verified. High efficiency transposase-mediated insertion
371 of the PiggyBac transposon cassette was accomplished through transient co-expression of the
372 mammalian optimized PiggyBac transposase (CMV HyPBase, (Yusa, et al., 2011)).

373

374 For multicolour labelling of subcellular structures, we utilized monomeric enhanced green
375 fluorescent protein (mEGFP) (gift from Karel Svoboda, Addgene plasmid #18696) (Harvey, et
376 al., 2008) and far-red mKate2 (Evrogen). These proteins were selected for their photostability,
377 low toxicity, high brightness and distinct emission spectra for dual-colour assays making them
378 suitable for live-cell imaging. To label the outer leaflet of the cell membrane, membrane-
379 associated palmitoylated proteins were generated by appending 20-amino acid sequence of
380 ratGAP-43 (MLCCMRRTKQVEKNDEDQKI) to the N-terminus (pm-XFP). To label the cell nucleus,
381 mEos3.2 and green-to-red photoconvertible protein (a gift from Michael Davidson & Tao Xu
382 (Addgene plasmid 54525) was coupled to Histone 2B (H2B) (Zhang, et al., 2012). For labeling of
383 filamentous actin, F-Tractin which contains the inositol triphosphate 3-kinase actin binding
384 domain was coupled to mKate2. Cell lines expressing both H2B-mEos3.2 and pm-mKate2 were
385 then created by co-transfection of each construct and selection for dual expressing cells using
386 FACS.

387

388 hPSCs transfection

389 H9 hESCs or hIPSCs were transfected using a Neon electroporator using 10 μl tips (Life
390 Technologies). Briefly, cells were dispersed, resuspended in TESR medium and counted as
391 described above. For each transfection 1e6 cells were collected by centrifugation at 300 xg for
392 2 minutes, washed with 1ml of PBS, then resuspended with 10μl of Neon electroporation buffer
393 R. 1 μg of piggyBac vector and 0.2 μg of CMV HyPBase vector was then added to the cells in a
394 volume of 2 μl. The cells were then electroporated (1150v, 30 mSec, 1 pulse), resuspended in
395 TESR medium supplemented with bFGF, Noggin and Y27632 and plated on Geltrex coated
396 dishes. Cells were maintained as described above then FAC-sorted 10 days after transfection.

397

398 Flow cytometry and cell sorting

399 Transfected hESCs or hiPSCs were dispersed and re-suspended as described above, then sorted
400 by FACS using a SH800 (Sony) cell sorter as a bulk pool of cells with a narrow gate selected for
401 robustly expressing cells. Quadrant gates used to estimate the percentage of positive cells and
402 level of fluorescence needed were designed based on fluorescence levels detected in the non-
403 transfected control samples. Sorted cells expressing medium levels of fluorescence were
404 expanded and frozen then representative lots of each cell line were thawed and tested for
405 mycoplasma contamination using the MycoAlert assay (Lonza), and fungi and aerobic bacteria
406 sterility by inoculating conditioned medium into trypticase soya broth (Sigma Aldrich). No
407 contamination was observed. In some instances (pm-eGFP in hIPSC4) monoclonal cell lines
408 were made from the polyclonal FACS sorted pools. To make monoclonal cell lines, 400 cells
409 were seeded into 60 mm dishes and cultured until the colonies were 2 – 3 mm in diameter.
410 They were then picked using 3.2 mm cloning discs (Sigma Aldrich) soaked in TrypLE select and
411 seeded into 96 well plates. Individual clones were then expanded in TESR medium. Controls
412 for pluripotency were undertaken as described above.

413

414 Neural differentiation assays

415 Spinal cord rosette differentiation: This was carried out following (Dady, et al., 2022, Verrier,
416 et al., 2018). Briefly, hESC were plated on Geltrex matrix (20 μg/cm2, Life Technologies) at a
417 density of 4e4 cells/cm^2 in TSER medium as described and allowed to attach for 24h. Cells were
418 differentiated for 48 hours in Neurobasal medium plus 1X B27, 1xN2, 1x non-essential amino
419 acids and 1x glutamax (all Thermo Fisher) (N2B27 medium) supplemented with 3 μM
420 Chiron99021 (Tocris) and 20 ng/ml bFGF (PeproTech) followed by a further 24 hours in N2B27
421 medium supplemented with 3 μM Chiron99021, 20 ng/ml bFGF, 10 μM SB431542 (Tocris) and
422 50 μg/ml Noggin (Peprotech) to obtain NeuroMesodermal progenitors (NMPs). For neural
423 differentiation of NMPs, these cells were then passaged using PBS-EDTA 0.5mM and seeded
424 back at controlled density (1e5 cells/cm2) on Geltrex (20μg/cm2, Life Technologies) in N2B27
425 medium supplemented with 10 μM SB431542, 50 μg/ml Noggin, 100 nM all-trans retinoic acid
426 (Sigma Aldrich) and 10 μM Y27632 (Tocris). After 24 hours the medium was removed and
427 replaced with N2B27 medium containing 100 nM all-trans retinoic acid for the remainder of
428 the differentiation. As described previously, dorsal spinal cord neural rosettes formed from day
429 6 (Dady, et al., 2022) and medium was refreshed every 3 days.

430

431 Forebrain/Cortical rosette differentiation: hPSCs were dispersed as described above, counted,
432 and re-suspended in TESR medium supplemented with bFGF (30 ng/ml), Noggin (10 ng/ml) and
433 Y27632 (10 μM) at a concentration of 1e5 cells/ml. 100 μl of cell suspension (1e4 cells) was
434 then added to the required number of wells of 96 well v-bottom plates and the cells pelleted
435 by centrifugation at 300 xg for 5 minutes to form embryoid bodies (EBs). EBs were cultured for
436 48 hours then collected from the 96 well plates using an 8-channel pipette, pooled together,
437 and washed twice with DMEM/F12 medium (Gibco). EBs were then resuspended in DMEM/F12
438 containing 20% knockout serum, 1x glutamax, 1x NEAA, 0.1 mM beta-mercaptoethanol (all
439 Gibco), SB431542 (10 μM, Tocris) and LDN193189 (0.5 μM Sigma Aldrich) and 50 EBs
440 transferred to each well of a low attachment 6-well plate in 2ml of medium to begin
441 differentiation. Every 48 hours 1ml of medium was removed from each well and replaced with
442 Neurobasal (Gibco) containing 1x glutamax, 1x NEAA, 1x N2 (Gibco), 1x B27 (Gibco), SB431542
443 (10 μM) and LDN193189 (0.5 μM). On day 9 of differentiation the EBs were recovered from the
444 6 well plates and replated on Geltrex coated (10 μg/cm2) 8 well chamber slides (Ibidi) using 10
445 – 15 EBs per well in Neurobasal containing 1x glutamax, 1x NEAA, 1x N2, 1x B27, SB431542 (10
446 μM) and LDN193189 (0.5 μM). The medium was refreshed every 48 hours until day 15 of
447 differentiation when it was changed to Neurobasal containing 1x glutamax, 1x NEAA, 1x N2, 1x
448 B27, BDNF (20 ng/ml, Peprotech) and GDNF (20 ng/ml, Peprotech). The medium was then
449 refreshed every 3 days, neural rosettes were evident from day 18 of differentiation.
450
451 Labeling individual cells in human spinal cord rosettes
452 For single cell or small cell group transfection, NMP-L cells were replated at end of D3 and
453 cultured for 8 to 9 days and transfected using Lipofectamine 3000 kit (Thermo Fisher) following
454 manufacturer's instructions with a combination of piggyBac plasmids (pm-eGFP + HypBase or
455 pm-mKate +H2B-mEos3.2 + HypBase) for a final concentration of 2 μg/μl of DNA mix. These
456 lipofected human neural progenitors were then cultured and imaged for the desired period.
457
458 Immunofluorescence
459 Commercially available primary antibodies were used to characterize cell types:
460 OCT4 Cell Signaling Technology (C30A3) rabbit mAb (1:400); SOX2 Cell Signaling Technology
461 (D6D9) rabbit mAb (1:400); NANOG Cell Signaling Technology (D73G4) rabbit mAb (1:400);
462 SSEA-4 Developmental Studies Hybridoma Bank (MC-813-70) mouse mAb (2 micro g per ml)
463 TRA-1-60 Cell Signaling Technology mouse mAb (1:200);TRA-1-81 Cell Signaling Technology
464 mouse mAb (1:200);SSEA-1 Developmental Studies Hybridoma Bank (MC-480) mouse mAb (2

465 micro g per ml);HNF-3 beta Cell Signaling Technology (D56D6) rabbit mAb (1:400) beta-III-
466 tubulin Sigma Aldrich (SDL.3D10) mouse mAb (1:800); Smooth muscle alpha actinin
467 Developmental Studies Hybridoma Bank (1E12) mouse mAb (2 micro g per ml); NCad, SIGMA,
468 1:500, PKC-ζ, Santa Cruz, SC-216; TBR2/EOMES 1:200 Abcam 23345, TUJ1, Covance Cat# MMS-
469 435P, mouse monoclonal 1:1000. hPSCs and neural rosettes were fixed in 1%
470 paraformaldehyde solution overnight at 4°C. Samples were then permeabilized with 0.1%
471 Triton X-100 in PBS and subjected to immunofluorescence labeling using appropriate
472 secondary antibodies conjugated to Alexa-fluor 488, 568 or 594 (Life Technologies), and
473 processed for DAPI staining to visualize cell nuclei. F-Actin cytoskeleton was labeled using
474 Phalloidin coupled with FITC fluorophore (1:1000; ThermoFisher). Fluorescence images were
475 taken on an EVOS Cell Imaging System (Thermo Fisher Scientific) for hPSCs, on a Leica SP8
476 confocal (using a 20X air or 63X NA1.2 APO water immersion objective) for spinal cord rosettes,
477 while cortical rosettes were imaged using LEICA SP8 Stellaris confocal microscope or a Zeiss
478 spinning disc confocal microscope equipped with a ×63 NA 1.4 oil immersion objective.
479
480 Generating satellite human spinal cord rosettes
481 From NMP cell passaging, transfected cells were cultured in N2B27 containing 100nM RA
482 (SIGMA) until day 6 when neural rosettes were easily observable. Using a very sharp glass
483 needle (0.29-0.31 mm) (Vitrolife), neural rosettes were individually micro-dissected and gently
484 deposited on a 35 mm glass bottom petri dish (WPI) previously coated with Geltrex (20µg/cm2,
485 Life Technologies). Micro-dissected rosettes were then cultured in N2B27 containing 100nM
486 RA (SIGMA) until the desired stage of observation.
487
488 Live imaging of human neural rosettes
489 Cells in satellite rosettes formed from primary micro-dissected spinal cord rosettes or individual
490 lipofected neural progenitors were imaged using a DeltaVision Core microscope system,
491 allowing detection of fine cellular detail at low fluorescence levels with minimal exposure time,
492 in a WeatherStation environmental chamber maintained at 37°C. The spinal cord rosette
493 culture medium was buffered with a 5% CO_2/95% air mix and maintained in a humid chamber.
494 Images were acquired using an Olympus 40x 1.30 NA objective using a Xenon light source and
495 a CoolSnap HQ2 cooled CCD camera (Photometrics). 30-40 optical sections (exposure time, 10-
496 50 milliseconds for each channel, 1024x1024 pixels, 2x2 binning) spaced 1.5µm apart were
497 imaged for each micro-satellite neural rosette at 10-minute intervals for periods up to 36h.
498 Images were deconvolved and maximum intensity projections of Z-stacks were made using

499 SoftWorx imaging software (Applied Precision) (Das, et al., 2012).

500 Confocal live imaging of cortical rosettes expressing F-Tractin::mKate2 was undertaken at 37°C
501 with a 5% CO_2/95% air mix using a Leica SP8 Stellaris confocal microscope with a x63 NA1.4 oil
502 objective. Stacks of 18 slices optical z-section separated by 0.8 µm, covering a 154×154×14.4
503 µm region were acquired over multiple positions every 310 seconds for up to 24 hours. We
504 applied a 3D gaussian blur with a sigma of 0.8x 0.8x 0.8 µm.

505 Quantification of cell behaviour

506 In spinal cord rosettes, apical visiting time was assessed by measuring time taken for a single
507 labelled cell located in the basal region of one spinal cord rosette (rosette periphery) to move
508 to the apical region and divide (rosette centre). To be consistent, observed rosettes were
509 selected by their similar diameter ~100-150 µm. At least 5 different cells per spinal cord rosette
510 and at least 5 different rosettes were analyzed for each time point (D13, D14, D18, 1D9).

511 Cell division symmetry was assessed by measuring the angle of the metaphase plate relative
512 to the apical surface at the lumen wall of the spinal rosette during cell division using Fiji. Cell
513 divisions were considered symmetric when the metaphase plate was perpendicular to the axis
514 of cell division. On the contrary, cell divisions were considered asymmetric when the
515 metaphase plate formed an angle of 40-45° to the axis of cell division (with one daughter cell
516 remaining longer at the apical surface. All cells were analysed in 3D. At least 5 different cells
517 per spinal cord rosette and at least 5 different rosettes were analyzed for each time point.

518 In cortical rosettes, we measured the time between cell cycle stages in rosettes expressing F-
519 Tractin-mKate2. Nuclear Envelope Breakdown was identified as the moment when cytoplasmic
520 F-Tractin entered the position held by the nucleus during the previous timepoint. Completion
521 of apical-to-basal migration as the moment when the cell appeared rounded at the apical
522 surface. Cytokinesis onset was defined as the timepoint when the first membrane cortical
523 contraction was detected. Cells in 12 different rosettes imaged for 22 hours from D29-D30
524 were analysed.

525 Statistical analysis

526 Statistical analysis for spinal cord rosettes was performed using non-parametric Mann-
527 Whitney U test for non-normally distributed data using Prism V8. Results are represented as
528 means ± SEM or SD as indicated in figures and p-values are indicated with *$p<0.05$, **$p<0.01$,
529 *** $p<0.001$, and ****$p<0.0001$.
530

Acknowledgements

The authors declare that they have no competing interests. We are grateful to Professor Timothy Sanders for gifts of APX-1 plasmid and FP-constructs. AD conducted also cloning work for some expression constructs in the Sanders Laboratory. This work was supported by an enhancement to a Wellcome Trust Investigator award to KGS (WT102817AIA). Research in the J.J. lab is supported by a BBSRC grant (BB/V001353/1). The Leica Stellaris microscope used for confocal live cell imaging was supported by BBSRC grant BB/T017546/1. The Leica SP8 was funded by a Wellcome Trust Multi-User Equipment grant (WT101468).

544 Figure Legends

545 Figure 1 Creation of fluorescent reporters in human pluripotent cells

546 A) Schematic of the APX1 plasmid used for high level expression of fluorescent protein fusion
547 constructs highlighting the relevant elements of the system; B) Schematic of fluorescent-
548 protein reporter constructs for introduction into human pluripotent cells using piggyBac
549 transposase; C) transfection regime and FACS for selection of cells expressing constructs; D)
550 Expression of reporters in human pluripotent cell lines, pm-eGFP, pm-mKate2, H2B-mEos3.2,
551 pm-mKate2::H2B-mEos or F-Tractin-pm-mKate2. Scale bars 50µm.

552

553 Figure 2 Spinal cord differentiation and rosette generation for live imaging

554 A) Neural differentiation regime, after (Verrier, et al., 2018) and primary neural rosette
555 formation and expansion from NMPs at (Day 4 to D14) apical/ luminal surface identified by N-
556 Cadherin (NCAD) expression, and nuclei by DAPI staining; B) manual microdissection of day 6
557 (D6) primary neural rosettes (PrR), replating and culture to 14/15 and beyond generates; C)
558 small satellite micro-rosettes (SmR) around the PrR, suitable for live imaging; D) Satellite
559 micro-rosette made using pm-eGFP hESC line (movie 1); E) selected frames from live imaging
560 of this SmR following IKNM including mitosis; F) Apical visiting time quantifications, revealing
561 increase as development progresses (5 independent experiments for each day, measurement
562 of 25 cells for each of D13 and D14, 23 cells for each of D18 and 19), means ± SD, p-values
563 *p<0.05, **p<0.01, *** p<0.001, and ****p<0.0001. Scale bars 50 µm

564

565 Figure 3 Mosaic transfection of spinal cord rosettes using lipofection

566 A) Timing of lipofection-mediated introduction of piggyBac constructs into spinal cord rosette
567 cells and live-cell imaging; B,C) pm-mKate2 construct expression revealing individual
568 neuroepithelial cell morphology across apico-basal axis; D,E) Mosaic pm-mKate2:H2B-mEOS3.2
569 expression allowing live-cell imaging of individual cells and facilitating measurement of division
570 symmetry (movie 2); and F) Percentage of asymmetric and symmetric divisions at apical surface
571 in individual rosettes during early and late D18-19 neurogenesis (5 independent experiments
572 for each stage: D13-14 (181 divisions in 26 rosettes), D18-19 (163 divisions in 36 rosettes)
573 means ± S.E.M; G,H) Live cell imaging of apical abscission in individual cell expressing the pm-
574 mKate:H2B-mEOS construct (movie 3). Scale bars 50 µm.

575

576

577

578 Figure 4 Live-cell imaging of F-Tractin in Cortical rosettes

579 Live imaging of cortical rosettes expressing F-Tractin showing, A) whole rosette monitored over
580 24h, note F-Tractin enrichment in apical end feet in rosette centre and prominent apical
581 mitoses (movie 4); B) Enrichment of F-Tractin::mKate2 at the apical tip of a delaminating cell (9
582 cases across 30 rosettes) (movie 5); C) Vertical cleavage plane (symmetric; n=101/110 divisions
583 occurring at the apical surface) division of a neuroepithelial cell in a cortical rosette. Values
584 above black arrows: average time between specific stages: respectively, n=83, n=98 and n=110
585 (movie 6); D) Horizontal cleavage plane (asymmetric; n=101/110 divisions occurring at the
586 apical surface) division of a neuroepithelial cell in a cortical rosette (movie
587 7); E) Neuroepithelial cell in a cortical rosette before and during Nuclear Envelope Breakdown
588 (NEB). Arrowheads: transient F-Tractin enrichment at basal nuclear surface; arrows: F-Tractin-
589 rich basal process (except in B, where indicates apical tip); asterisks: daughter cells following
590 cytokinesis. Scale bars: A), B), 20 µm, C), E), 10 µm, D) 5 µm, t0: NEB, all cortical rosette imaging
591 from D28 to 29.

592

593 Supplementary Figures

594 Figure S1 - FASC data for human pluripotent cells expressing fluorescent reporters
595 (related to Figure 1)

596 FASC data for selection of human pluripotent cells expressing fluorescent reporters, showing
597 expression of eGFP in 82.82% of cells, mKate2 in 92.74% of cells, and H2B-mEos3 only in 22.75%
598 of cells, while 13.79% of cells co-expressed pm-Kate and H2B-mEos3.2.

599

600 Figure S2 - Characterisation of cortical rosettes
601 (related to Figure 4)

602 A) Fixed cortical rosette stained for DAPI (magenta) and TBR2 (green); B) Fixed cortical rosette
603 stained for DAPI (blue), apically localised PKC-ζ (magenta) and neuronal Beta-Tubulin (green).
604 Lower panel: orthogonal re-slice. Scale bar: 50 µm; C) Fixed cortical rosette stained for
605 Phalloidin displaying similar localisation to F-tractin::mKate in Cortical rosette; D) Basal Cortical
606 progenitor cell division within the plane of the rosette (movie 8). Scale bars: A), B), C), 50 µm;
607 D) 20 µm (top) and 10 µm (bottom).

608

609

610

611

612 Movie legends

613 Live imaging of cell behaviour in human spinal cord rosettes

614 Movie 1 - related to Figs 2D ,E: example of nuclear apical-basal visiting in spinal cord rosette
615 expressing pm-eGFP

616 Movie 2 - related to Figs 3D ,E: examples of symmetric and asymmetric (final division) in spinal
617 cord rosette following lipofection-mediated mosaic expression pm-mKate2::H2B-mEos3.2

618 Movie 3 - related to Figs 3G, H: Apical delamination of individual neuroepithelial cell following
619 lipofection-mediated mosaic expression pm-mKate2::H2B-mEos3.2

620

621 Live imaging of cell behaviour in human Cortical rosettes

622 Movie 4 - related to Fig 4A: Live cortical rosette expressing F-Tractin-mKate2.
623 Scale bar: 20 µm.

624 Movie 5 - related to Fig 4B: Apical delamination of cortical progenitor cell. Scale bar: 10 µm.

625 Movie 6 - related to Fig 4C: Apical symmetrical division of cortical progenitor cell. Scale bar:
626 10 µm.

627 Movie 7 - related to Fig 4D: Apical asymmetric division of cortical progenitor cell.
628 Scale bar: 5 µm.

629 Movie 8 - related to Fig 4SD: Basal cortical progenitor cell division. Scale bars: 20 µm (top)
630 and 10 µm (bottom).

631

632

633 References

634 Booth, A. J. R., Yue, Z., Eykelenboom, J. K., Stiff, T., Luxton, G. W. G., Hochegger, H. and Tanaka, T. U.
635 (2019). Contractile acto-myosin network on nuclear envelope remnants positions human
636 chromosomes for mitosis. Elife 8.
637 Calegari, F., Haubensak, W., Haffner, C. and Huttner, W. B. (2005). Selective lengthening of the cell
638 cycle in the neurogenic subpopulation of neural progenitor cells during mouse brain development. J
639 Neurosci 25, 6533-6538.
640 Calegari, F. and Huttner, W. B. (2003). An inhibition of cyclin-dependent kinases that lengthens, but
641 does not arrest, neuroepithelial cell cycle induces premature neurogenesis. J Cell Sci 116, 4947-4955.
642 Cereseto, A. and Giacca, M. (2004). Integration site selection by retroviruses. AIDS Rev 6, 13-21.
643 Chambers, S. M., Fasano, C. A., Papapetrou, E. P., Tomishima, M., Sadelain, M. and Studer, L. (2009).
644 Highly efficient neural conversion of human ES and iPS cells by dual inhibition of SMAD signaling. Nat
645 Biotechnol 27, 275-280.
646 Charpentier, E. and Doudna, J. A. (2013). Biotechnology: Rewriting a genome. Nature 495, 50-51.
647 Dady, A., Davidson, L., Halley, P. A. and Storey, K. G. (2022). Human spinal cord in vitro differentiation
648 pace is initially maintained in heterologous embryonic environments. Elife 11.
649 Dambournet, D., Hong, S. H., Grassart, A. and Drubin, D. G. (2014). Tagging endogenous loci for live-cell
650 fluorescence imaging and molecule counting using ZFNs, TALENs, and Cas9. Methods Enzymol 546,
651 139-160.
652 Das, R. M. and Storey, K. G. (2014). Apical abscission alters cell polarity and dismantles the primary
653 cilium during neurogenesis. Science 343, 200-204.
654 Das, R. M., Wilcock, A. C., Swedlow, J. R. and Storey, K. G. (2012). High-resolution live imaging of cell
655 behavior in the developing neuroepithelium. Journal of visualized experiments : JoVE.
656 Davidson, P. M. and Cadot, B. (2021). Actin on and around the Nucleus. Trends Cell Biol 31, 211-223.
657 Ding, S., Wu, X., Li, G., Han, M., Zhuang, Y. and Xu, T. (2005). Efficient transposition of the piggyBac (PB)
658 transposon in mammalian cells and mice. Cell 122, 473-483.
659 Doudna, J. A. and Charpentier, E. (2014). Genome editing. The new frontier of genome engineering
660 with CRISPR-Cas9. Science 346, 1258096.
661 Elick, T. A., Bauser, C. A. and Fraser, M. J. (1996). Excision of the piggyBac transposable element in vitro
662 is a precise event that is enhanced by the expression of its encoded transposase. Genetica 98, 33-41.
663 Engelman, A. (2003). The roles of cellular factors in retroviral integration. Curr Top Microbiol Immunol
664 281, 209-238.
665 Felgner, P. L., Gadek, T. R., Holm, M., Roman, R., Chan, H. W., Wenz, M., Northrop, J. P., Ringold, G. M.
666 and Danielsen, M. (1987). Lipofection: a highly efficient, lipid-mediated DNA-transfection procedure.
667 Proc Natl Acad Sci U S A 84, 7413-7417.
668 Gunasekaran, S., Miyagawa, Y. and Miyamoto, K. (2022). Actin nucleoskeleton in embryonic
669 development and cellular differentiation. Curr Opin Cell Biol 76, 102100.
670 Hacein-Bey-Abina, S., Hauer, J., Lim, A., Picard, C., Wang, G. P., Berry, C. C., Martinache, C., Rieux-
671 Laucat, F., Latour, S., Belohradsky, B. H., et al. (2010). Efficacy of gene therapy for X-linked severe
672 combined immunodeficiency. N Engl J Med 363, 355-364.
673 Hacein-Bey-Abina, S., Von Kalle, C., Schmidt, M., McCormack, M. P., Wulffraat, N., Leboulch, P., Lim, A.,
674 Osborne, C. S., Pawliuk, R., Morillon, E., et al. (2003). LMO2-associated clonal T cell proliferation in two
675 patients after gene therapy for SCID-X1. Science 302, 415-419.
676 Harvey, C. D., Yasuda, R., Zhong, H. and Svoboda, K. (2008). The spread of Ras activity triggered by
677 activation of a single dendritic spine. Science 321, 136-140.
678 Haupt, A., Grancharova, T., Arakaki, J., Fuqua, M. A., Roberts, B. and Gunawardane, R. N. (2018).
679 Endogenous Protein Tagging in Human Induced Pluripotent Stem Cells Using CRISPR/Cas9. J Vis Exp.
680 Hockemeyer, D., Wang, H., Kiani, S., Lai, C. S., Gao, Q., Cassady, J. P., Cost, G. J., Zhang, L., Santiago, Y.,
681 Miller, J. C., et al. (2011). Genetic engineering of human pluripotent cells using TALE nucleases. Nat
682 Biotechnol 29, 731-734.
683 Hyrskyluoto, A. and Vartiainen, M. K. (2020). Regulation of nuclear actin dynamics in development and
684 disease. Curr Opin Cell Biol 64, 18-24.
685 Ivics, Z., Hackett, P. B., Plasterk, R. H. and Izsvak, Z. (1997). Molecular reconstruction of Sleeping
686 Beauty, a Tc1-like transposon from fish, and its transposition in human cells. Cell 91, 501-510.
687 Jinek, M., Chylinski, K., Fonfara, I., Hauer, M., Doudna, J. A. and Charpentier, E. (2012). A programmable
688 dual-RNA-guided DNA endonuclease in adaptive bacterial immunity. Science 337, 816-821.

689 Joung, J. K. and Sander, J. D. (2013). TALENs: a widely applicable technology for targeted genome
690 editing. Nat Rev Mol Cell Biol 14, 49-55.
691 Kasioulis, I., Dady, A., James, J., Prescott, A., Halley, P. A. and Storey, K. G. (2022). A lateral protrusion
692 latticework connects neuroepithelial cells and is regulated during neurogenesis. J Cell Sci 135.
693 Kasioulis, I., Das, R. M. and Storey, K. G. (2017). Inter-dependent apical microtubule and actin dynamics
694 orchestrate centrosome retention and neuronal delamination. Elife 6.
695 Kawakami, K. (2007). Tol2: a versatile gene transfer vector in vertebrates. Genome Biol 8 Suppl 1, S7.
696 Kawakami, K. and Shima, A. (1999). Identification of the Tol2 transposase of the medaka fish Oryzias
697 latipes that catalyzes excision of a nonautonomous Tol2 element in zebrafish Danio rerio. Gene 240,
698 239-244.
699 Kim, A. and Pyykko, I. (2011). Size matters: versatile use of PiggyBac transposons as a genetic
700 manipulation tool. Mol Cell Biochem 354, 301-309.
701 Lee, C. S., Bishop, E. S., Zhang, R., Yu, X., Farina, E. M., Yan, S., Zhao, C., Zheng, Z., Shu, Y., Wu, X., et al.
702 (2017). Adenovirus-Mediated Gene Delivery: Potential Applications for Gene and Cell-Based Therapies
703 in the New Era of Personalized Medicine. Genes Dis 4, 43-63.
704 Lee, C. Y., Li, J. F., Liou, J. S., Charng, Y. C., Huang, Y. W. and Lee, H. J. (2011). A gene delivery system for
705 human cells mediated by both a cell-penetrating peptide and a piggyBac transposase. Biomaterials 32,
706 6264-6276.
707 Lian, G. and Sheen, V. L. (2015). Cytoskeletal proteins in cortical development and disease: actin
708 associated proteins in periventricular heterotopia. Front Cell Neurosci 9, 99.
709 Liu, X., Li, N., Hu, X., Zhang, R., Li, Q., Cao, D., Liu, T., Zhang, Y. and Liu, X. (2013). Efficient production of
710 transgenic chickens based on piggyBac. Transgenic Res 22, 417-423.
711 Ludwig, T. E., Levenstein, M. E., Jones, J. M., Berggren, W. T., Mitchen, E. R., Frane, J. L., Crandall, L. J.,
712 Daigh, C. A., Conard, K. R., Piekarczyk, M. S., et al. (2006). Derivation of human embryonic stem cells in
713 defined conditions. Nat Biotechnol 24, 185-187.
714 Meyer, E. J., Ikmi, A. and Gibson, M. C. (2011). Interkinetic nuclear migration is a broadly conserved
715 feature of cell division in pseudostratified epithelia. Curr Biol 21, 485-491.
716 Miller, J. C., Tan, S., Qiao, G., Barlow, K. A., Wang, J., Xia, D. F., Meng, X., Paschon, D. E., Leung, E.,
717 Hinkley, S. J., et al. (2011). A TALE nuclease architecture for efficient genome editing. Nat Biotechnol
718 29, 143-148.
719 Miskey, C., Izsvak, Z., Plasterk, R. H. and Ivics, Z. (2003). The Frog Prince: a reconstructed transposon
720 from Rana pipiens with high transpositional activity in vertebrate cells. Nucleic Acids Res 31, 6873-
721 6881.
722 Narayanavari, S. A., Chilkunda, S. S., Ivics, Z. and Izsvak, Z. (2017). Sleeping Beauty transposition: from
723 biology to applications. Crit Rev Biochem Mol Biol 52, 18-44.
724 Norden, C., Young, S., Link, B. A. and Harris, W. A. (2009). Actomyosin is the main driver of interkinetic
725 nuclear migration in the retina. Cell 138, 1195-1208.
726 Okuno, T., Li, W. Y., Hatano, Y., Takasu, A., Sakamoto, Y., Yamamoto, M., Ikeda, Z., Shindo, T., Plessner,
727 M., Morita, K., et al. (2020). Zygotic Nuclear F-Actin Safeguards Embryonic Development. Cell Rep 31,
728 107824.
729 Olivera-Martinez, I., Schurch, N., Li, R. A., Song, J., Halley, P. A., Das, R. M., Burt, D. W., Barton, G. J. and
730 Storey, K. G. (2014). Major transcriptome re-organisation and abrupt changes in signalling, cell cycle
731 and chromatin regulation at neural differentiation in vivo. Development 141, 3266-3276.
732 Pacesa, M., Pelea, O. and Jinek, M. (2024). Past, present, and future of CRISPR genome editing
733 technologies. Cell 187, 1076-1100.
734 Rayon, T., Stamataki, D., Perez-Carrasco, R., Garcia-Perez, L., Barrington, C., Melchionda, M., Exelby, K.,
735 Lazaro, J., Tybulewicz, V. L. J., Fisher, E. M. C., et al. (2020). Species-specific pace of development is
736 associated with differences in protein stability. Science 369.
737 Roberts, B., Haupt, A., Tucker, A., Grancharova, T., Arakaki, J., Fuqua, M. A., Nelson, A., Hookway, C.,
738 Ludmann, S. A., Mueller, I. A., et al. (2017). Systematic gene tagging using CRISPR/Cas9 in human stem
739 cells to illuminate cell organization. Mol Biol Cell 28, 2854-2874.
740 Sanders, T. A., Llagostera, E. and Barna, M. (2013). Specialized filopodia direct long-range transport of
741 SHH during vertebrate tissue patterning. Nature 497, 628-632.
742 Sarkar, A., Sim, C., Hong, Y. S., Hogan, J. R., Fraser, M. J., Robertson, H. M. and Collins, F. H. (2003).
743 Molecular evolutionary analysis of the widespread piggyBac transposon family and related
744 "domesticated" sequences. Mol Genet Genomics 270, 173-180.
745 Sauer, F. C. (1935). Mitosis in the neural tube. J. Comp. Neurol. 62, 377-405.

Sheen, V. L., Jansen, A., Chen, M. H., Parrini, E., Morgan, T., Ravenscroft, R., Ganesh, V., Underwood, T., Wiley, J., Leventer, R., et al. (2005). Filamin A mutations cause periventricular heterotopia with Ehlers-Danlos syndrome. Neurology 64, 254-262.

Spear, P. C. and Erickson, C. A. (2012). Interkinetic nuclear migration: a mysterious process in search of a function. Dev Growth Differ 54, 306-316.

Sultana, T., Zamborlini, A., Cristofari, G. and Lesage, P. (2017). Integration site selection by retroviruses and transposable elements in eukaryotes. Nat Rev Genet 18, 292-308.

Szigeti, K., Ihnatovych, I., Rosas, N., Dorn, R. P., Notari, E., Cortes Gomez, E., He, M., Maly, I., Prasad, S., Nimmer, E., et al. (2023). Neuronal actin cytoskeleton gain of function in the human brain. EBioMedicine 95, 104725.

Takahashi, T., Nowakowski, R. S. and Caviness, V. S., Jr. (1995). The cell cycle of the pseudostratified ventricular epithelium of the embryonic murine cerebral wall. J Neurosci 15, 6046-6057.

Verrier, L., Davidson, L., Gierlinski, M., Dady, A. and Storey, K. G. (2018). Neural differentiation, selection and transcriptomic profiling of human neuromesodermal progenitor-like cells in vitro. Development 145.

Wang, W., Lin, C., Lu, D., Ning, Z., Cox, T., Melvin, D., Wang, X., Bradley, A. and Liu, P. (2008). Chromosomal transposition of PiggyBac in mouse embryonic stem cells. Proc Natl Acad Sci U S A 105, 9290-9295.

Woltjen, K., Michael, I. P., Mohseni, P., Desai, R., Mileikovsky, M., Hamalainen, R., Cowling, R., Wang, W., Liu, P., Gertsenstein, M., et al. (2009). piggyBac transposition reprograms fibroblasts to induced pluripotent stem cells. Nature 458, 766-770.

Wood, A. J., Lo, T. W., Zeitler, B., Pickle, C. S., Ralston, E. J., Lee, A. H., Amora, R., Miller, J. C., Leung, E., Meng, X., et al. (2011). Targeted genome editing across species using ZFNs and TALENs. Science 333, 307.

Woodard, L. E. and Wilson, M. H. (2015). piggyBac-ing models and new therapeutic strategies. Trends Biotechnol 33, 525-533.

Wu, S. C., Meir, Y. J., Coates, C. J., Handler, A. M., Pelczar, P., Moisyadi, S. and Kaminski, J. M. (2006). piggyBac is a flexible and highly active transposon as compared to sleeping beauty, Tol2, and Mos1 in mammalian cells. Proc Natl Acad Sci U S A 103, 15008-15013.

Yanakieva, I., Erzberger, A., Matejcic, M., Modes, C. D. and Norden, C. (2019). Cell and tissue morphology determine actin-dependent nuclear migration mechanisms in neuroepithelia. J Cell Biol 218, 3272-3289.

Yusa, K., Rad, R., Takeda, J. and Bradley, A. (2009). Generation of transgene-free induced pluripotent mouse stem cells by the piggyBac transposon. Nat Methods 6, 363-369.

Yusa, K., Zhou, L., Li, M. A., Bradley, A. and Craig, N. L. (2011). A hyperactive piggyBac transposase for mammalian applications. Proc Natl Acad Sci U S A 108, 1531-1536.

Zhang, M., Chang, H., Zhang, Y., Yu, J., Wu, L., Ji, W., Chen, J., Liu, B., Lu, J., Liu, Y., et al. (2012). Rational design of true monomeric and bright photoactivatable fluorescent proteins. Nat Methods 9, 727-729.

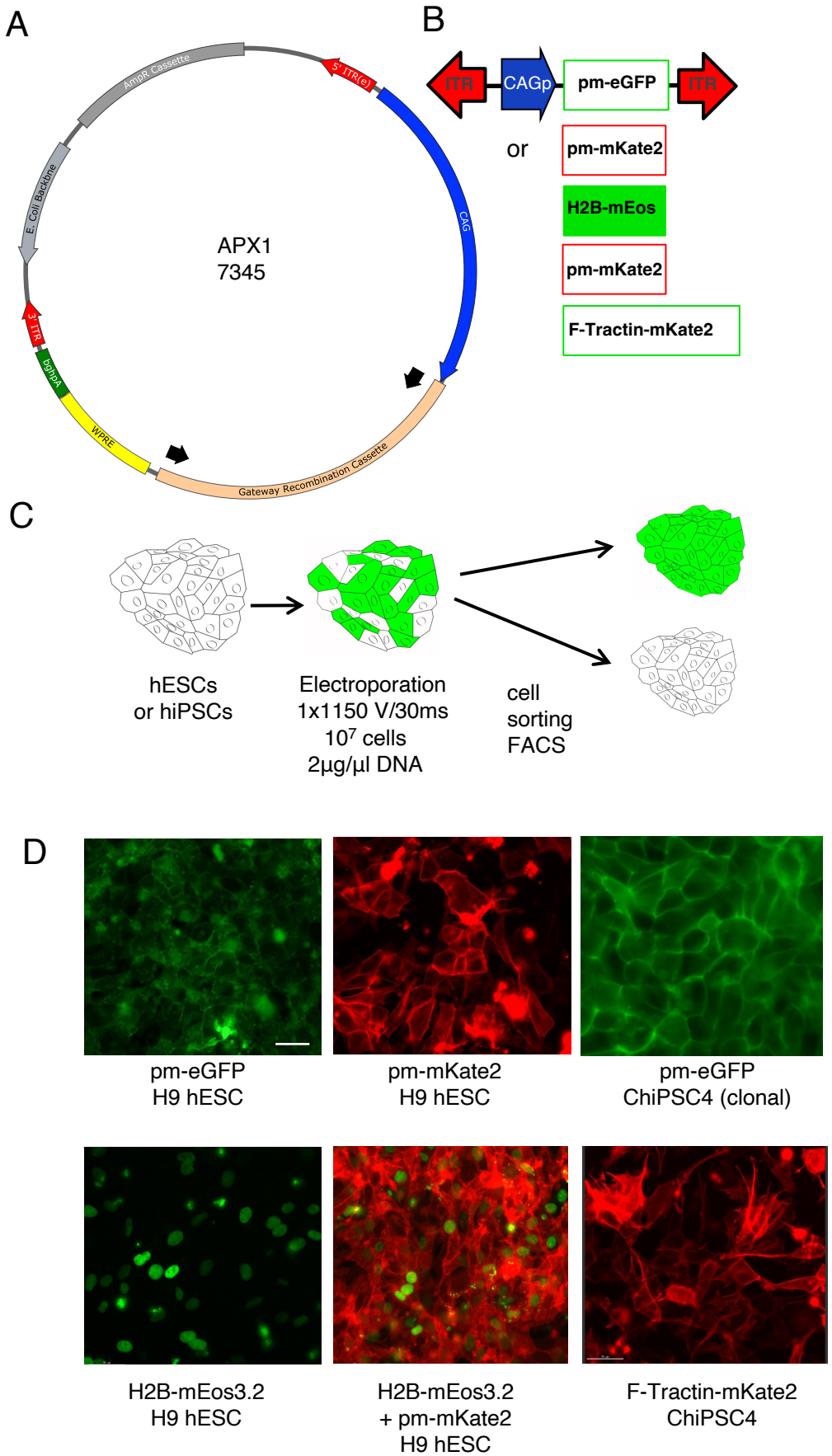

Figure 1 Dady et al

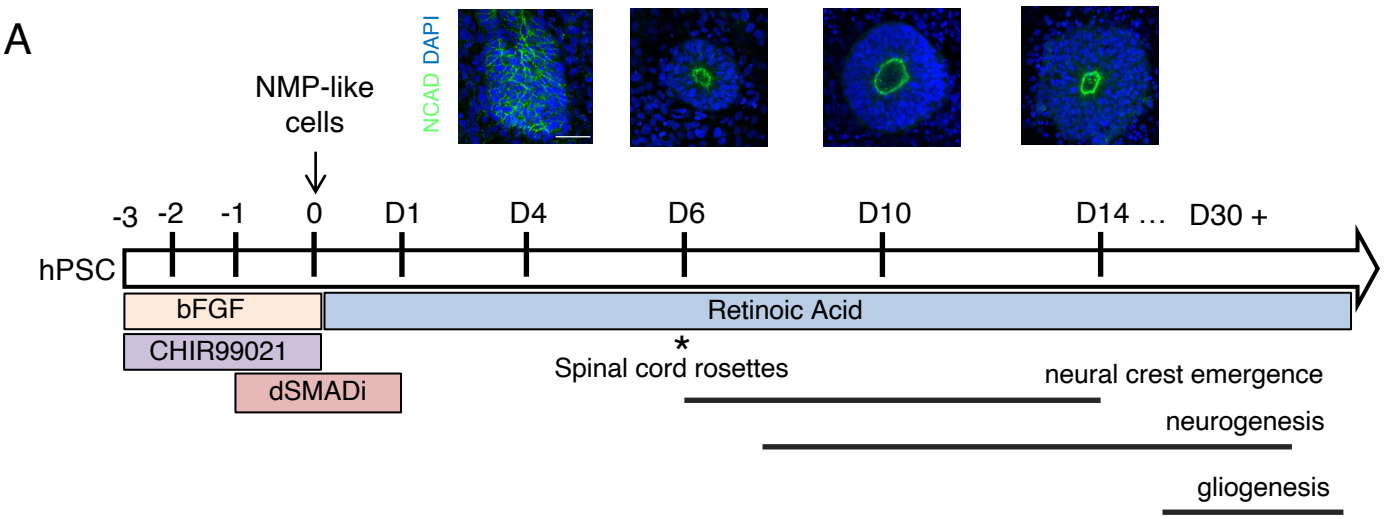

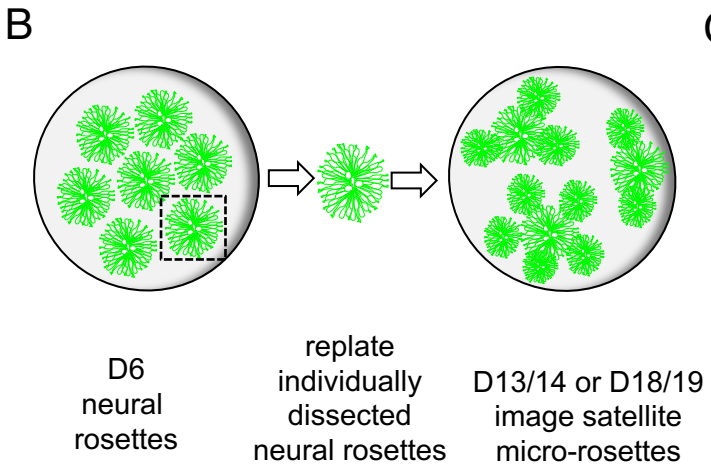

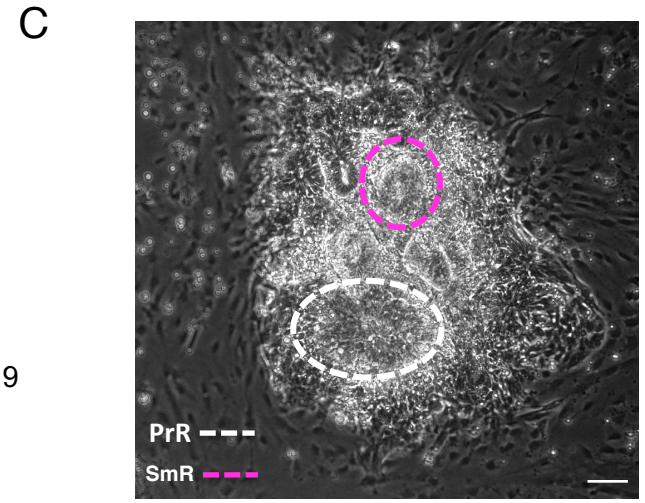

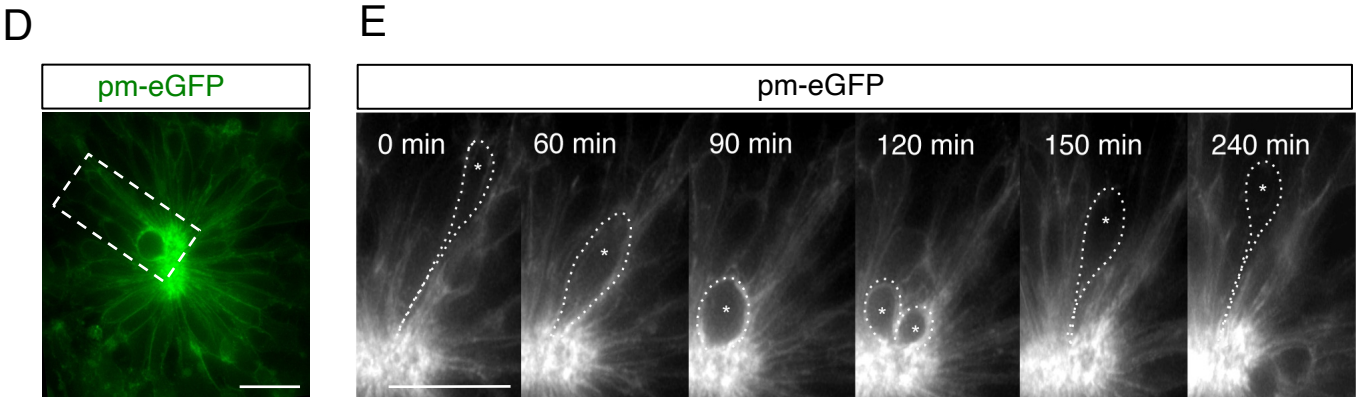

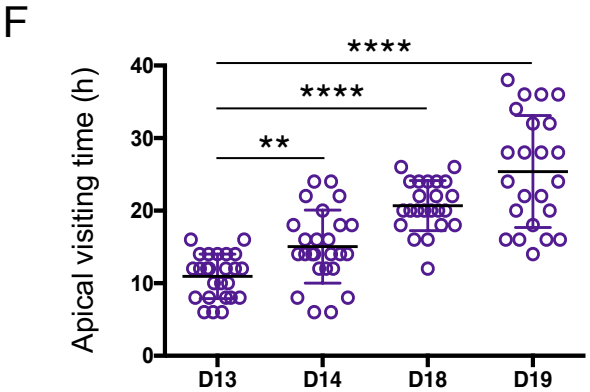

Figure 2 Dady et al

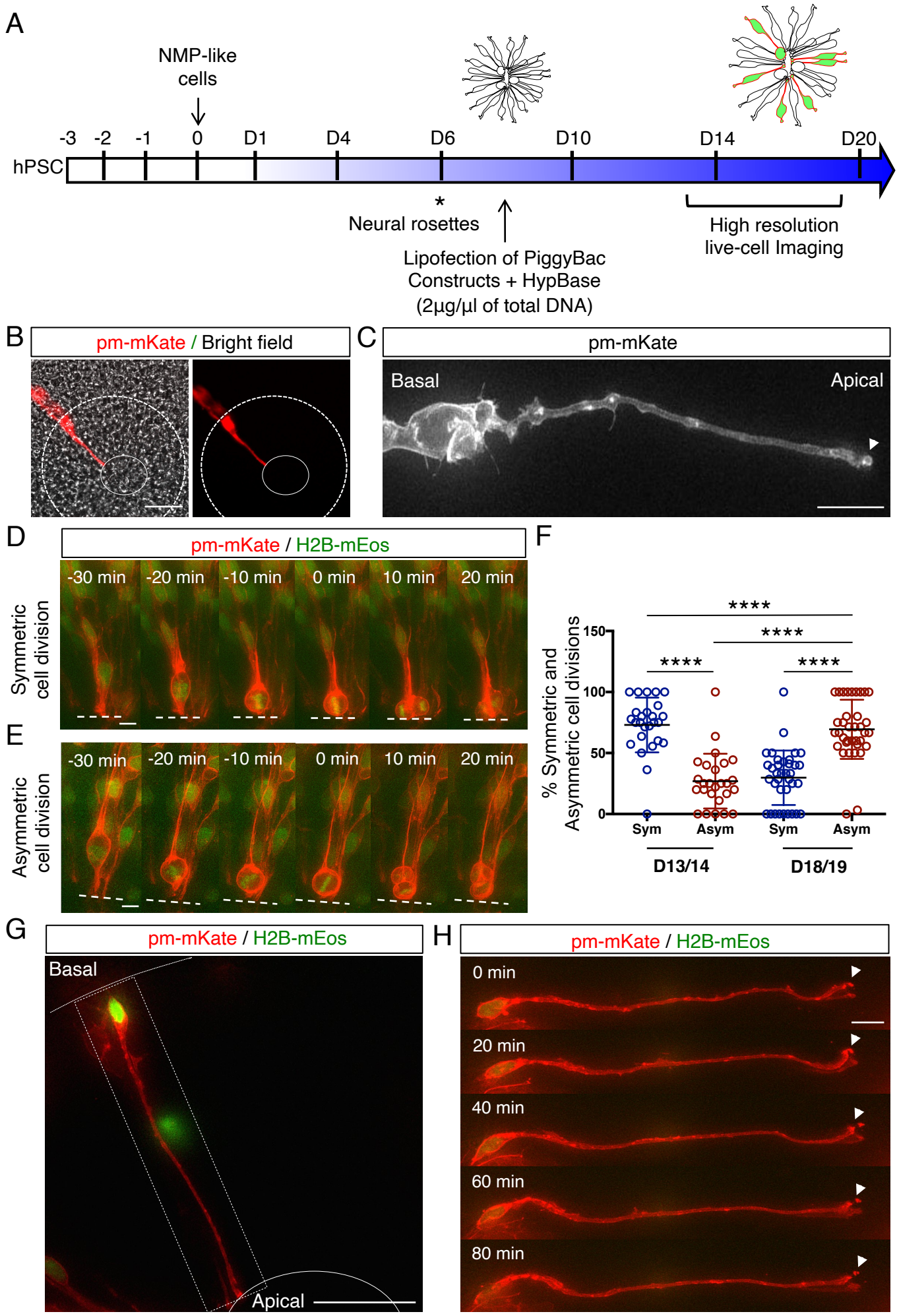

Figure 3 Dady et al

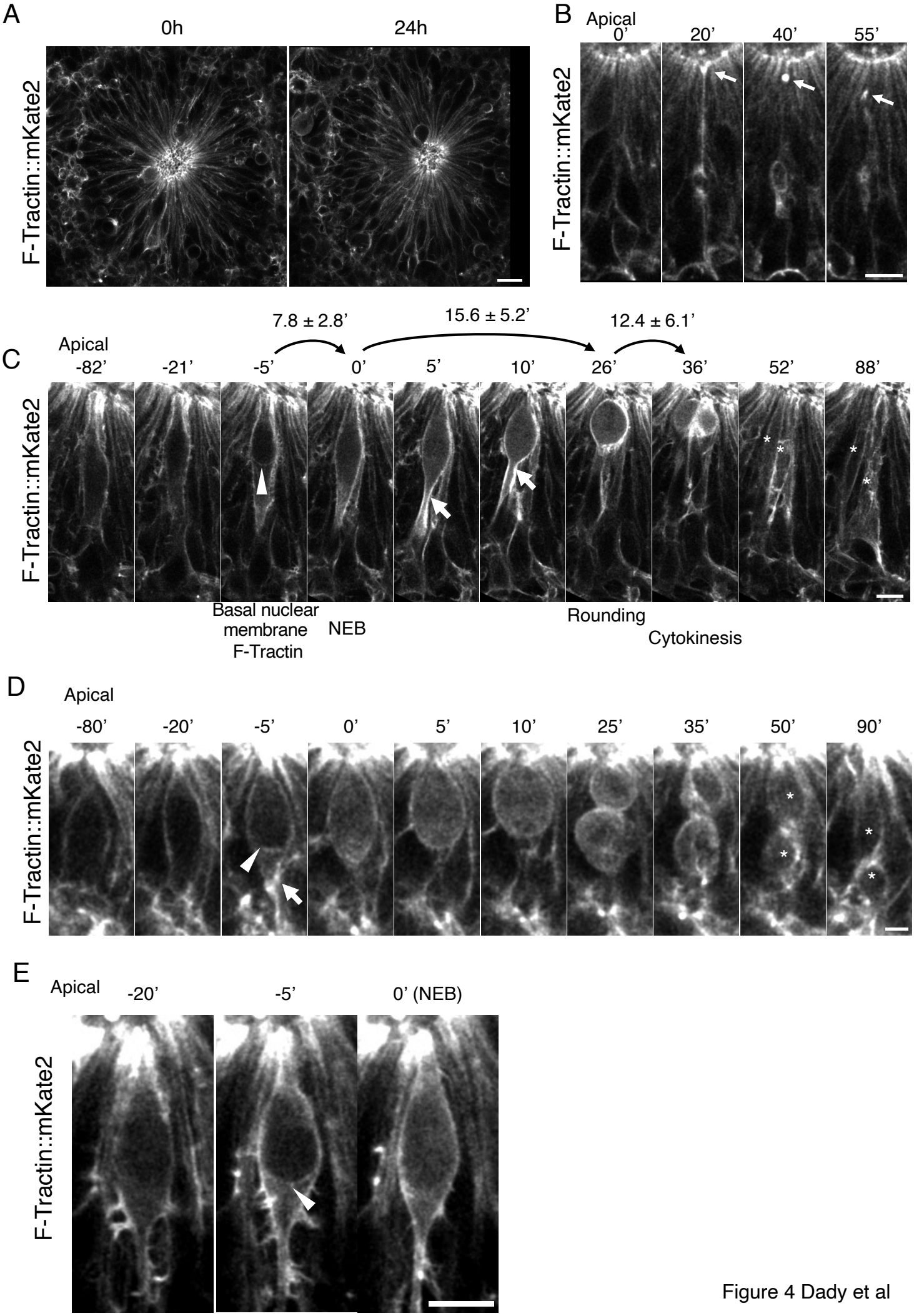

Figure 4 Dady et al

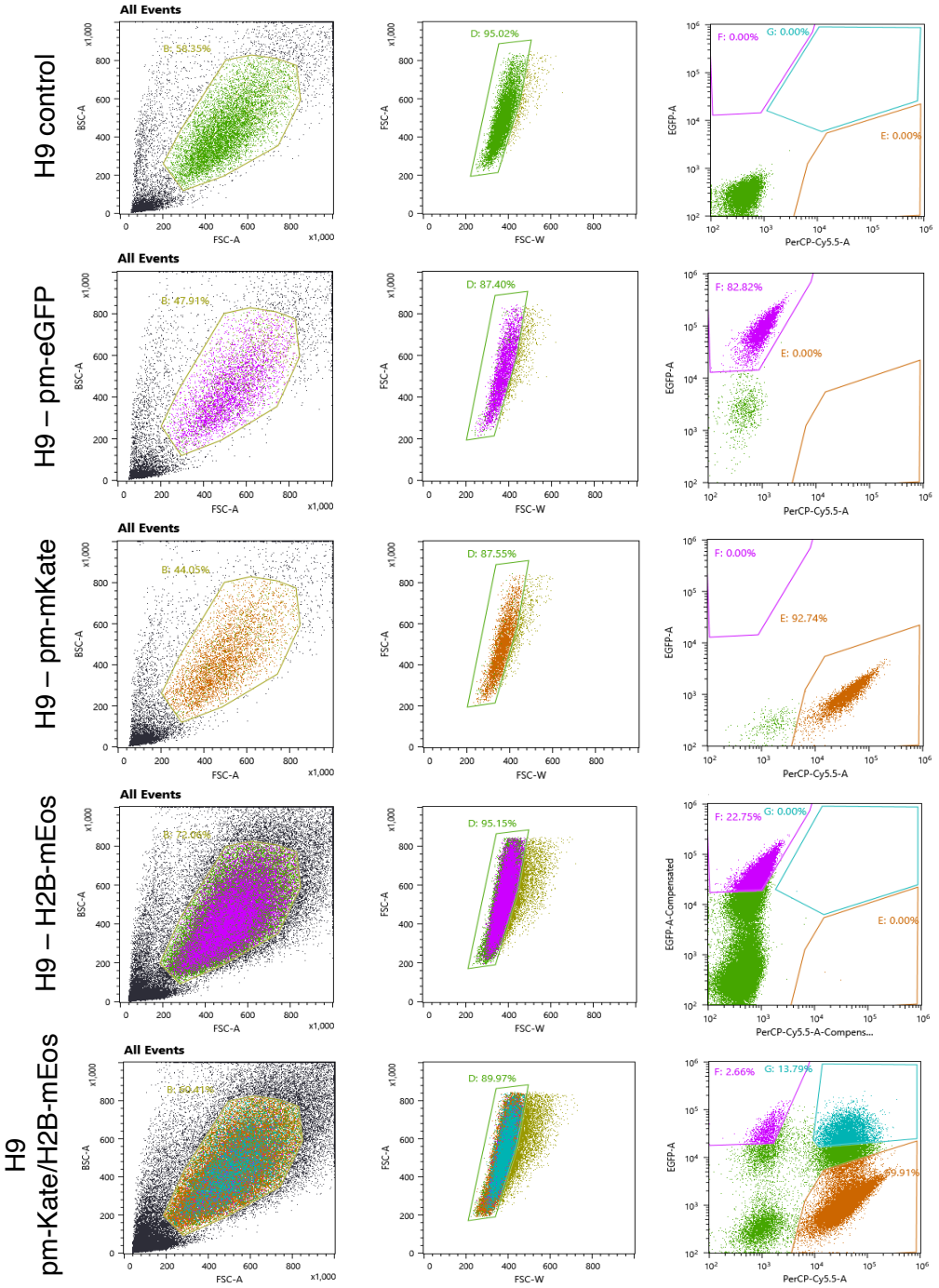

Figure S1 Dady et al

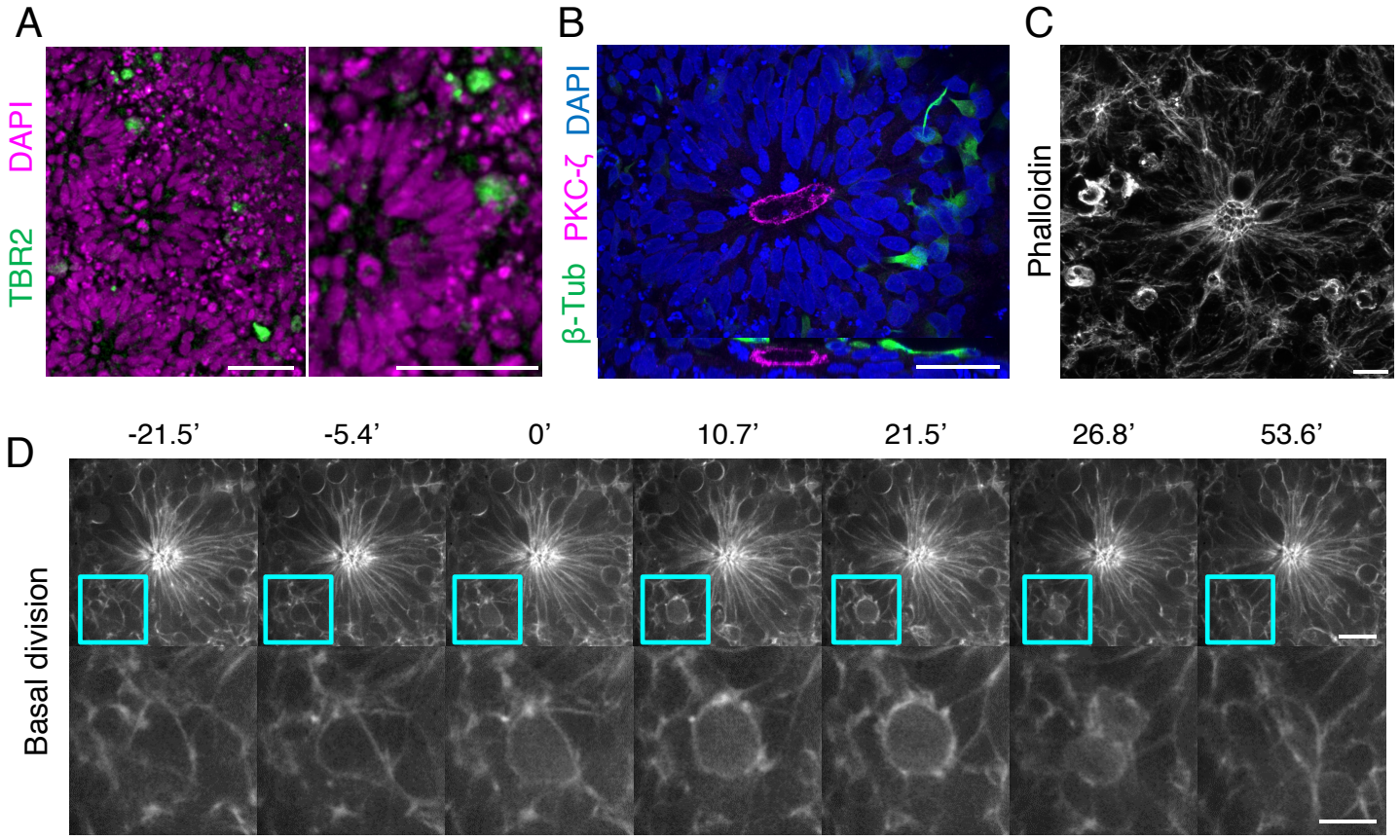

Dady et al Figure S2